Stem Cell Research & Therapy

https://doi.org/10.1186/s13287-026-04895-9

Article in Press

Hypoxia-conditioned BMSC exosomes improve short-term spinal cord injury outcomes via the miR-615-3p/PDE4C-mediated cAMP/PKA pathway

Received: 23 May 2025

Accepted: 2 January 2026

Published online: 12 January 2026

Cite this article as: Bian W., Zeng X., Liu Z. *et al.* Hypoxia-conditioned BMSC exosomes improve short-term spinal cord injury outcomes via the miR-615-3p/PDE4C-mediated cAMP/PKA pathway. *Stem Cell Res Ther* (2026). https://doi.org/10.1186/s13287-026-04895-9

Wei Bian, Xiangyu Zeng, Ziwen Liu, Mingyan Guan, Tegeleqi Bu, Haoze Li, Zewei Gao & Jianyu Liu

Hypoxia-conditioned BMSC exosomes improve short-term spinal cord injury outcomes via the miR-615-3p/PDE4C-mediated cAMP/PKA pathway

Wei Bian[1], Xiangyu Zeng[1], Ziwen Liu[1], Mingyan Guan[2], Tegeleqi Bu[1], Haoze Li[3], Zewei Gao[1], Jianyu Liu[1]*

[1]Department of Orthopedic Surgery, The Second Affiliated Hospital of Harbin Medical University, Harbin, Heilongjiang 150001, China

[2]Department of Orthopaedics, Northeast International Hospital, Shenyang, Liaoning 110000, China

[3]Department of Orthopaedics, The Fifth Hospital of Harbin, Harbin, Heilongjiang 150040, China

Corresponding Author:Jianyu Liu, MD, PhD,Department of Orthopedic Surgery, The Second Affiliated Hospital of Harbin Medical University

Address: Xuefu Road 246, Nangang District, Harbin, Heilongjiang 150001, China

Phone/Fax: +86-451-86605151

Email: liujianyu4@163.com

Abstract

Spinal cord injury (SCI) remains a significant global health challenge with limited effective therapeutic options. Exosomes derived from mesenchymal stem cells (MSCs) have emerged as promising neuroprotective agents due to their biocompatibility and immunomodulatory properties. This study investigated the therapeutic potential of hypoxia-conditioned bone marrow MSC (BMSC)-derived exosomes in both in vitro and in vivo SCI models. Hypoxic preconditioning significantly enriched miR-615-3p in bone marrow mesenchymal stem cell (BMSC)-derived exosomes. In

spinal neuron injury models, hypoxic exosomes enhanced cell viability, reduced apoptosis, and ameliorated dysfunction of the mitochondria-associated endoplasmic reticulum membranes (MAMs). Mechanistically, miR-615-3p directly targeted and suppressed phosphodiesterase 4C (PDE4C), activating the cyclic adenosine monophosphate (cAMP)/protein kinase A (PKA) pathway. This in turn modulated calcium signaling, attenuated mitochondrial calcium overload, and reduced endoplasmic reticulum stress (ERS). In a mouse model of SCI, short-term treatment with hypoxic exosomes promoted functional recovery within a 14-day post-injury period, as evidenced by improved locomotor performance, reduced lesion volume, attenuated tissue edema, and decreased inflammatory cell infiltration. Furthermore, in vivo administration of hypoxic exosomes upregulated miR-615-3p and downregulated PDE4C expression in injured spinal cord tissues. These results demonstrate that hypoxia-conditioned BMSC-derived exosomes exert neuroprotective effects via the miR-615-3p/PDE4C axis, highlighting their potential as a novel therapeutic strategy for SCI by targeting calcium homeostasis and mitochondrial-ER dysfunction. These findings demonstrate the short-term therapeutic potential of hypoxia-conditioned exosomes in SCI. However, further preclinical studies, including long-term follow-up to assess the durability of recovery and potential late-onset effects, alongside clinical validation, are warranted before clinical translation.

Keywords: Spinal cord injury; Hypoxia conditioning; Bone marrow mesenchymal stem cells; Exosomes; miR-615-3p; Neuroprotective effects

1. Introduction

Spinal cord injury (SCI) is a devastating neurological condition with an annual global incidence of approximately 900,000 cases, leading to severe motor, sensory, and autonomic deficits that impose a profound burden on individuals and society [1-3]. The pathophysiology of SCI encompasses both primary mechanical damage and a complex secondary injury cascade. This secondary phase is characterized by a self-perpetuating cycle of neuroinflammation, oxidative stress, and apoptotic signaling, which collectively exacerbate tissue destruction and impede axonal regeneration [4,5]. Key cellular events include microglial and astrocytic activation, driven partly by immunogenic myelin debris from white matter injury, which amplifies the inflammatory response [6,7]. Recent evidence further underscores the critical role of mitochondrial-associated endoplasmic reticulum membranes (MAMs), which serve as hubs for calcium signaling and redox homeostasis. Dysfunctional mitochondria-associated endoplasmic reticulum membranes (MAMs) contribute to endoplasmic reticulum stress (ERS), NLRP3 inflammasome activation, and neuronal apoptosis [8-10]. Microglial NLRP3 signaling has been identified as a key mediator of remote neuronal damage post-SCI [11], while non-coding RNAs fine-tune glial activity, adding layers of regulatory complexity [12,13].

Current therapeutic strategies, including pharmacotherapy, surgery, and rehabilitation, offer limited neurological recovery, particularly in elderly populations, and are often associated with significant adverse effects [14,15]. This underscores the urgent need for innovative and more effective treatments. In recent years, extracellular vesicles (EVs), especially exosomes derived from mesenchymal stem cells (MSCs), have emerged as promising therapeutic agents due to their biocompatibility, low immunogenicity, and ability to shuttle bioactive molecules, including proteins and nucleic acids, to recipient cells [16]. MSC-derived exosomes can modulate neuroregeneration, suppress inflammation, and promote angiogenesis, demonstrating significant neuroprotective potential [17,18]. However, challenges related to sourcing, purity, and therapeutic consistency hinder their clinical translation.

Hypoxic preconditioning has been explored as a strategy to enhance the therapeutic efficacy of MSC-derived exosomes. Hypoxia alters the exosomal cargo, including the enrichment of specific microRNAs (miRNAs), which are pivotal regulators of gene expression and represent promising therapeutic targets for SCI [19]. Specific microRNA species demonstrate therapeutic potential by

modulating inflammatory pathways [20]. For instance, hypoxia can significantly upregulate neuroprotective miRNAs, such as miR-615-3p, within exosomes, suggesting novel therapeutic strategies for SCI [21,22]. Nevertheless, the precise mechanisms by which hypoxia modulates specific exosomal miRNAs and their functional impacts in SCI remain inadequately characterized.

While several anti-inflammatory approaches have been investigated, including pharmacological inhibition of phosphodiesterase 4B/D (PDE4B/D) in neuroinflammatory disorders such as Alzheimer's and Parkinson's diseases [22,23], their efficacy in acute SCI remains limited. In contrast, PDE4C is predominantly expressed in neurons, suggesting its potential as a neuron-specific target. This study investigates how hypoxic preconditioning modifies BMSC exosomes, particularly through the enrichment of miR-615-3p, and explores their neuroprotective effects in spinal neuron injury models. We identify the miR-615-3p/PDE4C axis as a novel, neuron-specific mechanism that modulates calcium signaling and mitochondrial-ER dysfunction, offering a targeted therapeutic strategy distinct from broader anti-inflammatory approaches.

2. Materials and Methods

This study adheres to the Animal Research: Reporting of In Vivo Experiments (ARRIVE) guidelines 2.0. The completed ARRIVE Essential 10 checklist is provided as Supplementary File 2.

2.1.1 Experimental Animals

C57BL/6J mice (RRID:IMSR_JAX:000664) (6 weeks old, Jiangsu Huachuang Xinnuo Pharmaceutical Technology Co., Ltd.) were selected as experimental subjects.For BMSC isolation, donor mice of unspecified sex were used, as the primary focus of this study was on the effects of hypoxic preconditioning rather than donor sex. All in vivo therapeutic experiments were conducted using female mice.All animal procedures were conducted in accordance with relevant ethical guidelines.

Animal Anesthesia and Euthanasia

All surgical procedures and animal manipulations were performed under deep anesthesia to minimize suffering.

(1) Anesthesia: Mice were anesthetized with isoflurane for surgical operations. Eye lubrication and body temperature maintenance were ensured during anesthesia.

(2) Euthanasia and Tissue Preparation for Histology: At experimental endpoints, animals were deeply anesthetized and transcardially perfused with ice-cold phosphate-buffered saline (PBS) followed by 4% paraformaldehyde (PFA) in PBS. The spinal cord tissues were then carefully dissected and post-fixed in the same fixative for 24 hours at 4°C before further processing for histological analysis.

(3) Determination of Experimental Endpoints and Humane Endpoints: The predetermined experimental endpoints for tissue collection and analysis were post-injury day (PID) 3 and PID 14, as specified in the study design (Sections 2.6.1 and 2.7). These time points were selected to capture key phases of the secondary injury process and early recovery.

Humane endpoint monitoring was performed daily during the post-operative care period (as detailed in Section 2.6.1) to minimize animal suffering. Animals meeting any of the following criteria before a scheduled endpoint would have been euthanized immediately:

- Inability to access food or water, resulting in a body weight loss of >20% from baseline.
- Presence of severe autotomy (self-mutilation) of the hindlimbs.
- Development of severe systemic infection (e.g., ulcerative dermatitis, profound lethargy).

- Persistent convulsions or signs of extreme distress (e.g., unrelieved vocalization, self-mutilation) that are unresponsive to analgesia.
- Severe and persistent urinary dysfunction unresponsive to supportive care. Specifically, if an animal shows no improvement in urinary retention (e.g., anuria, significant abdominal distension) after at least 48-72 hours of consistent manual bladder expression and supportive therapy, and this is accompanied by a progressive decline in overall condition (e.g., profound lethargy, >20% body weight loss), indicating that its welfare cannot be maintained.
- Signs of systemic shock, including hypothermia (core body temperature < 32°C), severe dehydration (assessed by skin tenting), or profound lethargy unresponsive to external stimuli.

Throughout the study, none of the animals met these criteria for premature euthanasia, and all survived until their designated endpoints.

(4) Ethical Compliance: All procedures conformed to the approved protocol ("Mechanism of BMSC-Derived Exosomes in Spinal Cord Injury Repair," SYDW2024-111) and complied with the Chinese Regulations for the Administration of Laboratory Animals (2017 Revision) and the Harbin Medical University Animal Welfare Guidelines.

2.1.2 Key Reagents and Instruments

Reagents: Bone marrow mesenchymal stem cell (BMSC)-specific medium, Dulbecco's Modified Eagle Medium (DMEM), fetal bovine serum (FBS), and related cell culture supplements were used for cell culture. Primary antibodies included rabbit anti-CD63 (RRID:AB_2878298), rabbit anti-CD9 (RRID:AB_2877955), and

mouse anti-calnexin (RRID:AB_2069006). Key functional assays were performed using commercial kits for exosome isolation, protein and RNA analysis, and cell transfection (e.g., Lipofectamine 3000). Suppliers, catalog numbers, and detailed working concentrations for all reagents are comprehensively listed in Supplementary Table S1.

Instruments: Experimental procedures utilized a cell culture incubator, inverted microscope, centrifuge, biosafety cabinet, microplate reader, fluorescence and confocal microscopes, a spinal cord impactor, transmission electron microscope, nanoparticle tracking analyzer, and an in vivo imaging system. Manufacturers and model numbers for all instruments are provided in Supplementary Table S1.

2.2.3 BMSC Isolation and Culture

To obtain high-quality bone marrow mesenchymal stem cells (BMSCs), the following protocol was employed:

Experimental Steps:

(1) The biosafety cabinet was ultraviolet-sterilized for 30 minutes. Mice were euthanized and disinfected in 70% ethanol for 5-10 minutes.

(2) Femurs and tibias were rapidly isolated and placed in sterile PBS containing antibiotics.

(3) Residual muscles were removed, and bone ends were trimmed to expose the marrow cavity.

(4) A 5 mL syringe filled with 4 mL complete medium (DMEM + 10% FBS + 1% penicillin-streptomycin) was used to flush bone marrow into a Petri dish. The cell suspension was gently pipetted 15 times

for uniform distribution.

(5) The suspension was layered over an equal volume of mouse lymphocyte separation solution in a 15 mL centrifuge tube and centrifuged at 1500 rpm for 20 minutes.

(6) Mononuclear cells from the intermediate cloudy layer were transferred to a new tube, washed twice with DMEM, and centrifuged at 1000 rpm for 5 minutes.

(7) The supernatant was discarded, and cells were resuspended in BMSC-specific medium (hasenbio HS-C-003), seeded at 1×10^5 cells/cm² in T75 flasks, and cultured at 37°C with 5% CO_2.

(8) Complete medium changes were performed every 3 days starting on day 5 until 80-90% confluency.

(9) Adherent cells were subcultured at a 1:2 ratio upon reaching 80-90% confluency. Passage 3 cells were used for experiments to ensure consistency.

2.2 Exosome Isolation and Characterization

Cell Source: BMSCs were isolated from C57BL/6J mice (as described in Section 2.1.1) and used for exosome production. The sex of the donor mice for BMSC isolation was not specified, and future studies will be needed to investigate the potential impact of donor sex on exosomal cargo and therapeutic efficacy.

2.2.1 Isolation Protocol

(1) Cell Culture and Hypoxic Preconditioning: BMSCs at passage 3 were cultured in DMEM/F12 medium (hasenbio, HS-C-003) supplemented with 10% FBS at 37°C under 5% CO_2. Upon reaching 80–90% confluency, the culture medium was replaced with exosome-depleted FBS-containing DMEM/F12

medium (hasenbio, HS-C-003). For hypoxic preconditioning, cells were transferred to a three-gas incubator (Thermo Scientific, model 8000) and maintained at 1% O_2, 5% CO_2, and balanced N_2 at 37°C for 24 hours. Normoxic control cells were cultured under standard conditions (21% O_2, 5% CO_2) for the same duration.

(2) Collection and Clarification of Conditioned Medium: Following incubation, the conditioned medium from both groups was collected and centrifuged at 3000 × *g* for 10 minutes at 4°C to remove cellular debris and apoptotic bodies.

(3) Exosome Isolation: The clarified supernatant was subjected to exosome isolation using a commercial kit (see Supplementary Table S1) according to the manufacturer's instructions. Note that kit-based isolation may co-isolate non-exosomal particles such as protein aggregates or lipoproteins.

(4) Purification and Quantification: Isolated exosomes were resuspended in PBS and further purified by ultracentrifugation at 100,000 × *g* for 70 minutes to minimize co-isolation of contaminants. The final exosome pellet was resuspended in PBS, and the protein concentration was quantified using the BCA Protein Assay Kit.

2.2.2 Characterization Methods

(1) **Transmission Electron Microscopy (TEM):** Exosome suspensions were applied to copper grids, negatively stained with phosphotungstic acid, and observed under an 80 kV Hitachi HT7700 TEM. The characteristic cup-shaped morphology of exosomes was confirmed.

(2) Nanoparticle Tracking Analysis (NTA): Particle size

distribution and concentration were analyzed using a ZetaView PMX 110 instrument. Each sample was measured at least three times, with each run lasting no less than 60 seconds. The particle number was normalized to the exosomal protein concentration (determined by BCA assay) to report particles per μg protein.

(3) Western Blot: Expression of exosomal markers (CD63, CD9) and absence of the endoplasmic reticulum marker calnexin were verified using specific antibodies (anti-CD63, RRID:AB_2878298; anti-CD9, RRID:AB_2877955; anti-calnexin, RRID:AB_2069006). For detailed antibody information, refer to Supplementary Table S1.

(4)Exosome Uptake Assay: PKH67-labeled exosomes were co-incubated with neurons (stained with DAPI) and visualized under a Leica TCS SP8 confocal microscope (63× objective). To rule out non-specific uptake from dye micelles or aggregates, control experiments were performed with PKH67 dye alone (without exosomes) and with exosomes disrupted by 1% Triton X-100 before labeling. No significant fluorescence was observed in these controls, confirming specific exosome uptake.

2.3 Construction of Spinal Neuron Cell Injury Model

2.3.1 H_2O_2-Induced Oxidative Stress

The human spinal neuronal cell line (RRID:CVCL_IZ28) was exposed to 200 μmol/L H_2O_2. Cell line and reagent sources are detailed in Supplementary Table S1.

2.3.2 Exosome Intervention

Exosomes from the hypoxic group (hypoxic exosomes) and normoxic control group (Normoxia-Exo) were resuspended in PBS,

filter-sterilized, and added to the injury model at a concentration of 100 μg/mL. After co-culture for 24 hours, subsequent assays were performed. We hypothesized that hypoxic exosomes would significantly improve neuronal cell viability, reduce apoptosis, and regulate calcium signaling, exerting protective effects.

2.4 Spinal Neuron Injury Model

2.4.1 Cell Isolation: Primary spinal neurons were isolated from neonatal C57BL/6J mice (RRID:IMSR_JAX:000664). Spinal cords from neonatal C57BL/6J mice were dissociated into single-cell suspensions and cultured on poly-L-lysine-coated coverslips using neuronal medium (Sciencell #1521).

2.4.2 Injury Model:

(1) Lipopolysaccharide (LPS; Sigma, #L6529) was used to induce an inflammatory injury in spinal neurons.
(2) Injured cells were co-cultured with BMSC-derived exosomes under varying conditions to evaluate neuroprotective effects.

2.5 Cell Function Assays

2.5.1 CCK8 Assay: Spinal neurons were seeded in 96-well plates, incubated with exosomes for 48 hours, and analyzed at 450 nm using a Diatek DR-3518GL microplate reader.

2.5.2 Hoechst 33342/PI Staining: Apoptosis was assessed by staining cells with Hoechst 33342 and propidium iodide (PI), followed by visualization under a fluorescence microscope.

2.5.3 Mitochondria-Associated Endoplasmic Reticulum Membrane (MAMs) Structure Analysis: MitoTracker Red and an

antibody against calnexin (Proteintech, #66903-1-Ig, RRID:AB_2882143) were used to label mitochondria and endoplasmic reticulum (ER), respectively. Structural changes in mitochondria-associated endoplasmic reticulum membranes (MAMs), which are critical sites for calcium signaling and lipid exchange, were observed via confocal microscopy.

2.5.4 Ca^{2+} Imaging: Cytosolic and mitochondrial calcium levels were assessed using specific fluorescent probes according to the manufacturers' instructions.

(1) Cytosolic Ca^{2+} Measurement: Spinal neurons were loaded with 5 μmol/L Fluo-3 AM (Beyotime, #S1056) in serum-free medium at 37°C for 30 minutes. After washing with PBS to remove excess dye, the fluorescence intensity (Ex/Em = 488/525 nm) was immediately observed and captured using an Olympus IX71 fluorescence microscope.
(2) Mitochondrial Ca^{2+} Measurement: Cells were loaded with 2 μmol/L Rhod-2 AM (Beyotime, #S2060) at 37°C for 30 minutes. Following incubation and PBS washes, the fluorescence intensity (Ex/Em = 552/581 nm) was detected to indicate mitochondrial calcium levels.
For both assays, at least three independent experiments were performed, and fluorescence intensity was quantified using ImageJ software (NIH, USA) from at least 30 cells per group in each experiment.

2.6 SCI Animal Model

2.6.1 Model Construction:

(1)Female C57BL/6J mice (RRID:IMSR_JAX:000664) (8 weeks old) were used to establish the SCI model. This choice was made to preclude potential aggression and fighting-related injuries among group-housed male mice during the extended post-operative recovery period, thereby minimizing confounding variables and ensuring animal welfare.
(2)Post-injury care, monitoring, and supportive therapy: Animal health, welfare, and humane endpoints were monitored at least

twice daily during the first 3 post-operative days and at least once daily thereafter until the endpoint. This monitoring cadence was aligned with the administration of supportive medications. The monitoring included assessment of body condition, spontaneous activity, posture, wound condition, and signs of pain or distress. Analgesia was provided via subcutaneous injection of buprenorphine (0.1 mg/kg) every 8-12 hours for the first 48 hours. Antibiotic prophylaxis (gentamicin, 5 mg/kg, subcutaneous) was administered daily for 14 days.
To manage common post-SCI complications, bladder dysfunction was addressed by manual expression of the urinary bladder twice daily. Bladder expression was performed whenever the bladder was palpably distended, or if no urination was observed for over 12 hours, to prevent overdistension and rupture. The primary goal of this supportive care was to maintain the animal's welfare and prevent the development of conditions meeting humane endpoint criteria. Euthanasia was only considered when such persistent and intensive supportive measures failed to stabilize the animal's condition, and it continued to exhibit signs of severe distress or progressive decline. Prophylaxis against constipation included the provision of a hydrated gel diet and monitoring of stool output. Subcutaneous saline was administered if dehydration was suspected or stool output ceased. These daily care routines also served as scheduled times for the formal assessment of humane endpoints.
(3)Spinal cord tissues were harvested following transcardial perfusion with 4% PFA at the designated time points (e.g., PID 3 and 14) for subsequent histological and immunohistochemical analyses.

2.6.2 Exosome Administration:

Fluorescently labeled exosomes (BMSC-exos or Hypo-BMSC-exos) were administered via tail vein injection to track their biodistribution. In vivo imaging system (IVIS, PerkinElmer) quantified exosome biodistribution.

For therapeutic efficacy studies, mice received a single tail vein injection of 200 µL PBS containing 200 µg exosomal protein (derived from either BMSC-exos or Hypo-BMSC-exos) immediately (0 hours) after SCI. Based on the particle-to-protein ratios

determined by NTA (Section 2.2.2), this dose corresponds to approximately 1.04×10^{12} particles for hypoxic exosomes and 1.00×10^{12} particles for normoxic exosomes. Assuming an average mouse body weight of 20 g, this equates to approximately 5.2×10^{10} and 5.0×10^{10} particles per gram body weight, respectively. The rationale for this single immediate dosing was supported by our IVIS tracking data (Fig. 6A-B), which confirmed robust accumulation of intravenously injected exosomes at the spinal cord lesion site within 24 hours, suggesting a critical early window for therapeutic intervention. This dosing strategy is consistent with previously reported effective regimens in rodent models of central nervous system injury [24,25]. It should be noted that while the immediate (0-hour) administration was effective in our model, delayed dosing or repeat dosing regimens were not systematically evaluated in this study, which warrants future investigation to define the optimal therapeutic window.

2.6.3 Neurologic Assessment of Motor Function:

Neurologic assessment was performed by two independent investigators who were blinded to the treatment groups. Group assignments were concealed using a computer-generated random number sequence, and the blinding was maintained until all behavioral and histological analyses were completed. The investigators were formally trained in the scoring criteria prior to the experiment. Assessments were conducted at baseline and on post-injury days (PID) 1, 3, 7, and 14 in a dedicated behavioral testing room under consistent conditions.

(1) Basso, Beattie, Bresnahan (BBB) Locomotor Rating Scale [26]:

Mice were placed individually in a circular open-field arena (50 cm in diameter, 30 cm high walls) and allowed to move freely for 4 minutes. The arena was cleaned with 70% ethanol between trials to eliminate olfactory cues. Hindlimb movements (including joint motion, weight support, plantar stepping, coordination, and trunk stability) were observed and scored by two blinded investigators according to the 22-point BBB scale (0: no observable hindlimb movement; 21: normal gait). The final score for each mouse was the average of both observers' scores. Any discrepancies were resolved through re-evaluation to reach a consensus.

(2) Footprint Analysis:

A straight runway (constructed from transparent Plexiglas, 50 cm length × 5 cm width × 10 cm height) was used. The forepaws and hindpaws of the mice were coated with non-toxic, water-soluble red and blue ink (Shanghai Yi Sheng Biotechnology, China), respectively, using a fine brush. Mice were then gently guided to walk along the runway, leaving a continuous trail of footprints on white absorbent paper covering the runway floor. Each mouse underwent three independent trials. Trials were excluded a priori if the footprints were smudged, the run was discontinuous, or the mouse stopped or deviated from the runway. For each valid trial, at least three consecutive and clear step cycles were analyzed using ImageJ software (NIH, USA). The values from the three trials were then averaged to obtain a single value for each parameter per mouse. The following parameters were quantified:

Stride Length (mm): The distance between the centers of two consecutive paw prints of the same hindpaw.

Base of Support (mm): The perpendicular distance between the centers of the left and right hindpaw prints.

Regularity Index (%): The percentage of normal step sequence

patterns out of the total number of steps.

The protocols for spinal cord tissue collection, processing, and the analysis of histopathology and inflammatory severity are described in detail in Sections 2.7 and 2.8.4.

2.6.4 Randomization and Experimental Unit

（1）Randomization Procedure:

Animals were randomly assigned to experimental groups (Sham, SCI, SCI+BMSC-exos, SCI+Hypo-BMSC-exos) using a computer-generated random number sequence. The randomization was performed by an investigator not involved in the surgical procedures, behavioral assessments, or data analysis to ensure allocation concealment. Group assignments were concealed until the completion of all experiments.

（2）Definition of Experimental Unit:

The experimental unit for each analysis was defined as follows:

① For behavioral assessments (e.g., BBB scale, footprint analysis), the experimental unit was the individual animal.

② For histological analyses (e.g., H&E staining, LFB staining, immunofluorescence), the experimental unit was the spinal cord section from each animal, with multiple fields analyzed per section.

③ For molecular analyses (e.g., qPCR, Western blot, ELISA), a subset of animals was randomly allocated for these assays due to tissue limitations. Specifically, for Western blot analysis (Fig. 8C-D), n = 3 biologically independent animals per group. For qPCR and ELISA analyses (Fig. 8A-B), n = 5 biologically independent animals per group. The experimental unit for all molecular analyses was the tissue sample from each individual animal; no pooling of samples from multiple animals was performed.

④ For in vivo imaging and exosome tracking, the experimental unit was the individual animal.

This definition ensures that statistical analyses account for the appropriate level of replication and variability.

2.6.5 Primary and Secondary Outcome Measures

The primary and secondary outcome measures for this study were pre-specified prior to data collection and analysis.

(1) Primary Outcome:

Hindlimb locomotor function:Assessed using the Basso, Beattie, Bresnahan (BBB) Locomotor Rating Scale at baseline and on post-injury days (PID) 1, 3, 7, and 14.

(2) Secondary Outcomes:

①**Gait analysis parameters:**Stride length, base of support, and regularity index from footprint analysis on PID 14.

② **Histopathological measures:**Lesion volume, tissue edema severity, and inflammatory cell infiltration count from H&E staining.

③ **Myelin integrity:** Semi-quantitative assessment of myelin preservation from LFB staining.

④ **Molecular readouts:**

1)-Expression levels of miR-615-3p and PDE4C in spinal cord tissue (qPCR and Western blot)

2)Oxidative stress markers (ROS, MDA) and pro-inflammatory cytokines (TNF-α, IL-1β, IL-6) from ELISA

3)Mitochondrial-ER dysfunction markers (MAMs integrity, calcium levels, GRP78 expression)

4)cAMP/PKA pathway activation (cAMP levels, p-PKA/PKA ratio).

2.7 Spinal Cord Tissue Collection and Processing

At designated endpoints (PID 3 and 14), mice were deeply anesthetized and transcardially perfused with ice-cold PBS followed by 4% paraformaldehyde (PFA). Spinal cord segments encompassing the injury epicenter and adjacent regions were carefully dissected and post-fixed in 4% PFA for 24 hours at 4°C.

For histopathological analysis (H&E and LFB staining), tissues were subsequently dehydrated through a graded ethanol series, cleared in xylene, and embedded in paraffin. Serial longitudinal sections were cut at a thickness of 4 µm for staining.

For immunofluorescence analysis and other molecular studies, tissues were cryoprotected in 30% sucrose solution, embedded in OCT compound, and sectioned at 10 µm thickness using a cryostat.

For molecular analyses (e.g., Western blot, qPCR), fresh spinal cord tissues were snap-frozen in liquid nitrogen and stored at −80°C until use.

2.8 Data Analysis

2.8.1 RNA Processing: Total RNA was extracted using TRIzol and reverse-transcribed with a Vazyme MR101-02 kit.

2.8.2 qPCR: Real-time PCR (KCD-M1004 kit) was performed on a YRUI MA-600 system. Relative gene expression was calculated using the $2^{-}\Delta\Delta Ct$ method.

2.8.3 Western Blot: Protein quantification (Biosharp BL521A) preceded SDS-PAGE and PVDF membrane transfer. Blots were imaged using a Tianneng 5200 system.

2.8.4 Histopathological and Inflammatory Severity Analysis

The severity of inflammation and tissue damage was assessed

through complementary histopathological and biochemical methods.

(1) Histopathological Analysis: For histopathological evaluation, paraffin-embedded spinal cord tissues (as described in Section 2.7) were used. Serial longitudinal sections (4 µm thickness) were prepared and stained with Hematoxylin and Eosin (H&E) and Luxol Fast Blue (LFB) for myelin visualization.

H&E Staining: Sections were deparaffinized in xylene, rehydrated through a graded ethanol series, stained with hematoxylin for 3–5 minutes, differentiated in 1% HCl-75% ethanol, blued in alkaline water, and counterstained with eosin for 30–60 seconds. After dehydration and clearing, sections were mounted with neutral resin.

LFB Staining: After deparaffinization and rehydration, sections were stained in preheated LFB solution (Servicebio, G11030-100ML) at 65°C for 4 hours, rinsed, and differentiated sequentially in LFB differentiation solutions B and C until myelin was clearly visualized against a near-colorless background.

Histopathological evaluation was performed by two independent observers blinded to the treatment groups. The severity of inflammation was quantified by counting the number of infiltrating inflammatory cells in three random, non-overlapping high-power fields (400× magnification) per H&E-stained section using ImageJ software (NIH, USA). Tissue edema was assessed based on the separation of tissue architecture and the presence of clear spaces in H&E-stained sections. Myelin integrity was semi-quantitatively assessed in LFB-stained sections.

(2) Biochemical Analysis (ELISA): Levels of reactive oxygen species (ROS), malondialdehyde (MDA), and pro-inflammatory cytokines (TNF-α, IL-1β, IL-6) in spinal cord homogenates and

serum were measured using specific commercial ELISA kits according to the manufacturers' instructions. Absorbance was quantified at 450 nm using a microplate reader (Diatek, DR-3518GL).

2.9 Statistical Methods

2.9.1 Statistical Analysis

The experimental unit for each analysis was explicitly defined in Section 2.6.4. Data are presented as mean ± SD. Sample size calculation was performed using G*Power 3.1 software (α=0.05, power=0.8) to ensure adequate statistical rigor. The sample size calculation was based on the following assumptions: effect size f = 0.4 (medium-to-large effect based on preliminary experiments), test family = F-tests, statistical test = ANOVA: Fixed effects, omnibus, one-way. This effect size (f=0.4) was derived from pilot data (n=3 per group) assessing BBB scores at day 7 post-SCI, and the variance estimates in the pilot study were consistent with those observed in the present main experiment.For repeated measures analyses (e.g., BBB scores), we assumed a correlation among repeated measures of 0.5 and nonsphericity correction ε = 1. Consistent with Section 2.6.4, the unit of analysis for all in vivo data was the individual animal. This includes behavioral assessments, where n represents the number of animals, and molecular/histological analyses, where n represents the number of biologically independent tissue samples (each from a separate animal). These parameters yielded a required total sample size of 32 animals (8 per group) to achieve 80% power at α = 0.05. Comparisons between groups were analyzed by one-way ANOVA (for multi-group comparisons) or Student's t-test (for two-group

comparisons) using GraphPad Prism 9.0. Data distribution normality was verified using the Shapiro-Wilk test, and variance homogeneity was confirmed by Levene's test prior to parametric analysis. Non-parametric alternatives (Mann-Whitney U test or Kruskal-Wallis test) were applied when data violated normality assumptions. Significance thresholds were defined as $*p < 0.05$, $**p < 0.01$, and $***p < 0.001$. For all analyses involving repeated measures (detailed in Section 2.9.2), the same procedures for testing sphericity and handling violations were applied.For all bar graphs depicting quantitative data, values are presented as mean ± SD with individual data points overlaid to enhance transparency.

2.9.2 Statistical Analysis for Neurologic Assessments

Neurologic assessment data were analyzed as follows: BBB locomotor scores were analyzed using two-way repeated measures ANOVA with Bonferroni's post hoc test for multiple comparisons across time points (baseline, PID 1, 3, 7, 14) and treatment groups. The assumption of sphericity for the BBB score analysis was assessed using Mauchly's test. Where the assumption of sphericity was violated ($p < 0.05$), the Greenhouse-Geisser correction was applied to adjust the degrees of freedom. No missing data points were encountered in the behavioral assessments; thus, all animals contributed data at all pre-specified time points, and the analysis was performed on complete cases. Footprint analysis parameters (stride length, base of support, regularity index), which were assessed only at PID 14, were analyzed using one-way ANOVA with Bonferroni's post hoc test for comparisons between treatment groups. Statistical analyses were performed using GraphPad Prism 9.0.Normality of data distribution was verified using the

Shapiro-Wilk test, and homogeneity of variances was assessed using Levene's test. If data violated normality or homogeneity assumptions, non-parametric alternatives were applied (Friedman test followed by Dunn's multiple comparisons). Significance thresholds were defined as $*p < 0.05$, $**p < 0.01$, and $***p < 0.001$.

2.9.3 Image Analysis

Quantification of Western blot bands and immunofluorescence images was performed using ImageJ software (NIH, USA). For Western blot analysis, the optical density of each band was measured and normalized to the corresponding loading control (e.g., GAPDH). For immunofluorescence analysis (e.g., MAMs structure, colocalization studies), background subtraction using a fixed rolling ball radius of 50 pixels was applied uniformly, and the fluorescence intensity or Pearson's correlation coefficient for colocalization was calculated using the ImageJ plugin 'Coloc 2'.For colocalization analyses, thresholds were set manually using a uniform strategy and applied consistently across all images and groups; Costes' randomization was used to validate the analysis. Fields of view for analysis were selected systematically by acquiring images from at least three random, non-overlapping regions per specimen.All analyses were performed under consistent parameters, with a minimum of three fields or biological replicates sampled per specimen.For colocalization analysis of MAMs (e.g., MitoTracker Red and Calnexin), regions of interest (ROIs) were defined using a uniform thresholding strategy in ImageJ, applied consistently across all groups. The analysis was performed by an investigator blinded to the treatment groups to avoid bias.

2.9.4 Pre-specified Analysis Plan and Multiplicity Control

A pre-specified statistical analysis plan was established prior to data collection to control for multiple comparisons:

(1) Primary Outcome Analysis:

① BBB scores were analyzed using two-way repeated measures ANOVA with Bonferroni's post hoc test.

②This conservative approach controls the family-wise error rate for the primary outcome across all time points.

(2) Secondary Outcomes Analysis:

①For multiple secondary endpoints assessed at the same time point:

1)One-way ANOVA with Bonferroni's post hoc test was used for group comparisons.

2)Significance level was maintained at $\alpha=0.05$ for each pre-planned comparison.

② - For molecular and histological analyses performed at multiple time points (PID 3 and 14):

1)Separate analyses were conducted for each time point to avoid artificial inflation of sample size.

2)Bonferroni correction was applied when multiple related markers were analyzed simultaneously.

(3) Hierarchical Testing Approach:

①The primary outcome (BBB scores) was analyzed first.

② All secondary outcome families (including functional, histopathological, and molecular readouts) were gatekept by the significance of the primary outcome. That is, only if the primary outcome showed statistical significance were any secondary outcomes analyzed. This gatekeeping procedure applied to all pre-specified secondary outcome families, including functional (gait analysis), histopathological (lesion volume, inflammation, myelin integrity), and molecular readouts (miR-615-3p/PDE4C expression, oxidative stress markers, cytokines, and mitochondrial-ER

dysfunction markers).

③ This hierarchical approach minimizes the family-wise error rate across all outcome families while maintaining statistical power for key endpoints.

④Multiple Comparison Adjustment for Molecular Assays: For multiple molecular markers assessed simultaneously at the same time point (e.g., multiple cytokines in ELISA or multiple proteins in Western blot), the Holm-Bonferroni method was applied over the standard Bonferroni correction. This approach was chosen because it provides a better balance between Type I and Type II error rates in the context of correlated molecular outcomes, while still adequately controlling the family-wise error rate.

3. Results

3.1 Hypoxia conditioning significantly enhances miR-615-3p expression in BMSC exosomes

Hypoxic preconditioning significantly enriched miR-615-3p in both BMSCs and their derived exosomes, as evidenced by qPCR analysis with individual data points overlaid (**$p < 0.01$ for exosomes; ***$p < 0.001$ for BMSCs, Fig. 1D). Notably, hypoxia treatment did not alter the characteristic bilayer membrane structure observed via TEM (Fig. 1A), and NTA confirmed a preserved size distribution within the typical exosomal range (30–150 nm, Fig. 1B). Quantification revealed comparable particle-to-protein ratios between groups (hypoxic exosomes: 5.2×10^9 particles/μg; normoxic exosomes: 5.0×10^9 particles/μg), further confirming that hypoxic preconditioning did not compromise exosome integrity or yield. Western blot demonstrated robust and comparable expression of exosomal positive markers (CD63, CD9) and the

absence of the negative marker calnexin in both groups (Fig. 1C), confirming the purity of the isolated vesicles.

To verify the functional delivery of exosomal cargo, we performed an exosome uptake assay. Confocal microscopy confirmed the efficient internalization of PKH67-labeled hypoxic exosomes by spinal neurons, as shown by their co-localization with DAPI-stained nuclei (Fig. 1E). Control experiments with PKH67 dye alone or using Triton X-100-disrupted exosomes showed no significant fluorescence, confirming that the observed signal was due to specific exosome uptake and not non-specific dye incorporation. Notably, these control groups exhibited negligible fluorescence, reinforcing the specificity of exosome uptake observed in the experimental group.

Collectively, these comprehensive characterizations (TEM, NTA, WB) and the functional uptake assay confirm the successful isolation of intact exosomes and demonstrate that hypoxic preconditioning specifically enhances the packaging of miR-615-3p into these vesicles without altering their fundamental physical properties or uptake efficiency.

3.2 Protective effects of hypoxic exosomes in spinal neuron injury models

Treatment with hypoxic exosomes was associated with significantly improved cellular viability in vitro compared to Normoxia-Exo, as shown by CCK-8 assay with individual data points overlaid (*p <0.001, Fig. 3A). This was accompanied by a clear reduction in cell death, quantified by PI staining (p <0.01, Fig. 3B). Confocal microscopy revealed that hypoxic exosomes treatment attenuated cytosolic calcium levels (Fluo-3 AM staining, **p < 0.05, Fig. 3C)

and reduced mitochondrial calcium overload (Rhod-2 AM staining, *$p < 0.05$, Fig. 3D). Additionally, the treatment restored mitochondrial-associated ER membrane (MAM) integrity, as shown by immunofluorescence colocalization ($p < 0.01$, Fig. 4A-C).This was associated with altered expression and localization of key MAM-regulating proteins, including mitofusin 2 (MFN2) and dynamin-related protein 1 (DRP1) (Fig. 4B, C).

3.3 Critical role of miR-615-3p in mediating exosome neuroprotection

miR-615-3p mimic transfection potentiated the protective effects of hypoxic exosomes (CCK-8 assay, ***p <0.001, Fig. 2A), while inhibitor transfection partially reversed these benefits (*p <0.05, Fig. 2A). Dual-luciferase reporter assays confirmed direct binding between miR-615-3p and the Phosphodiesterase 4C (PDE4C) 3'UTR (*p <0.05, Fig. 5D-E), suggesting PDE4C as a functional target.

3.4 Short-term functional and histological improvements in SCI mice

(1) As the pre-specified primary outcome, intravenous administration of Hypo-BMSC-Exo significantly improved locomotor recovery in SCI mice, as evidenced by improved BBB scores across the 14-day observation period, with data presented as mean ± SD and individual data points overlaid (p <0.05, Fig. 6C).

(2)Assessment of secondary outcomes further demonstrated therapeutic benefits:

Gait analysis on post-injury day (PID) 14 revealed a significant increase in hindpaw stride length, also shown with overlaid data points (p <0.01, Fig. 6D).

Histological examination by H&E staining revealed multifaceted tissue protection... Quantitative analysis with overlaid data points demonstrated not only a reduced lesion area (p <0.01, Fig. 7A) but also a significant decrease in inflammatory cell infiltration (p <0.05, Fig. 7B).

Notably, an attenuation of tissue edema was observed compared to the control group (Fig. 7A–B). The alleviation of edema suggests a potential protective effect against vasogenic edema, a key pathological feature of secondary SCI.

These findings demonstrate the promising short-term therapeutic effects of hypoxic exosomes within the 14-day post-injury window. The observed significant improvement in the primary outcome (BBB locomotor scores), a validated measure of functional recovery in SCI models, coupled with the consistent benefits across multiple secondary histopathological assessments, collectively underscores the therapeutic relevance of our functional assessments.

These functional and histological improvements were paralleled by beneficial molecular changes, including the downregulation of pro-inflammatory cytokines (TNF-α, IL-6; Fig. 8A) and oxidative stress markers (ROS and MDA; Fig. 5A, 8A). This convergence of evidence—from locomotor recovery and gait analysis to structural preservation and anti-inflammatory effects—confirms that hypoxic exosomes confer comprehensive neuroprotection within the 14-day post-injury window.

3.5 Modulation of oxidative stress and inflammation by hypoxic exosomes

hypoxic exosomes treatment reduced spinal cord oxidative stress and systemic inflammation, as quantified with individual data

points overlaid for ROS levels (*p <0.05, Fig. 5A) and pro-inflammatory cytokines (TNF-α p <0.01, IL-6 *p <0.05, Fig. 8A). Concurrently, spinal miR-615-3p expression was upregulated (p <0.01, Fig. 5B) while PDE4C protein levels decreased (*p <0.05, Fig. 8B-D) in treated animals, with the qPCR data in Fig. 5B also presented using overlaid data points.

3.6 Mechanistic regulation of calcium signaling via the miR-615-3p/PDE4C axis

To delineate the mechanistic pathway, we first confirmed that miR-615-3p directly targets PDE4C using dual-luciferase reporter assays and RNA pull-down assays, with quantitative results presented with overlaid data points (Fig. 5D-E). Hypoxic exosome treatment led to significant suppression of PDE4C expression at both mRNA and protein levels (Fig. 5B-C). This suppression activated the cAMP/PKA pathway, as evidenced by elevated cAMP levels and an increased p-PKA/PKA ratio, both shown with individual data points overlaid (Fig. 7C-D). Consequently, downstream mitochondrial calcium overload was attenuated (Fig. 3C), and endoplasmic reticulum stress (ERS) was reduced, indicated by decreased GRP78 expression quantified with overlaid data points (Fig. 8E). Furthermore, mitochondrial-ER membrane (MAM) integrity was restored (Fig. 4A-C), demonstrating a coherent pathway from miR-615-3p enrichment to functional recovery via PDE4C/cAMP/PKA-mediated calcium homeostasis.

4. Discussion

Spinal cord injury (SCI), a devastating neurological disorder, presents significant therapeutic challenges due to the complexity of

its pathophysiology. Emerging evidence highlights the critical roles of neuroinflammation and neuronal apoptosis in secondary injury mechanisms, which profoundly impact neurological recovery [27]. The pathogenesis of SCI is characterized by extensive white matter damage, wherein immunogenic myelin debris drives a protracted and destructive inflammatory response [6, 7]. Against this pathophysiological backdrop, This study investigates the effects of hypoxia conditioning on BMSC exosome properties and miR-615-3p expression, subsequently analyzing their functional roles in spinal neuron injury models, offering novel therapeutic insights for SCI management.

Hypoxic preconditioning has emerged as a promising strategy to enhance the therapeutic potential of mesenchymal stem cell (MSC)-derived extracellular vesicles (EVs), particularly exosomes, for regenerative applications [28]. Prior research demonstrates that hypoxia significantly improves the efficacy of MSC-exosomes in myocardial infarction and cerebral ischemia models [29,30]. While previous studies primarily focused on quantitative and functional enhancements of exosomes, our work delves deeper by identifying hypoxia-induced changes in specific microRNA cargo (miR-615-3p) and elucidating its mechanistic contributions to SCI repair.

The pathophysiology of SCI involves the complex interaction between primary and secondary injury mechanisms.Our findings are consistent with the growing recognition that inflammation, oxidative stress, and ERS are interconnected in SCI pathology. Notably, MAMs serve as a structural and functional platform linking mitochondrial calcium overload, ROS production, and NLRP3 inflammasome activation [31,32]. While conventional anti-inflammatory strategies often aim for global cytokine

suppression or glial modulation, they typically lack neuron-specificity and fail to address core neuronal pathologies such as calcium dyshomeostasis. In contrast, our approach using hypoxic exosomes employs a neuron-targeted mechanism via the miR-615-3p/PDE4C axis. By suppressing PDE4C, they not only modulate cAMP/PKA signaling but also directly rectify calcium signaling and mitochondrial-ER integrity, thereby offering a more precise therapeutic strategy beyond broad immunomodulation. This neuron-centric strategy, targeting PDE4C, is not intended to supplant interventions aimed at glial cells or vascular integrity, but rather to complement them. The pathophysiology of SCI is multifaceted, involving concurrent neurodegeneration, neuroinflammation, and vascular dysfunction. While glial-modulating approaches address the inflammatory cascade, and vascular targets aim to preserve the blood-spinal cord barrier, our findings suggest that directly bolstering neuronal resilience to calcium dysregulation and mitochondrial-ER stress is a crucial and parallel avenue for intervention. The miR-615-3p/PDE4C axis offers this neuronal specificity, potentially creating a more permissive microenvironment for other repair processes to occur.This targeted, multi-level intervention may explain the superior neuroprotection we observed.

Notably, previous studies reported 2-3 fold increases in exosome secretion from hypoxic MSCs with augmented pro-angiogenic capacities [33]. Our findings reveal a 3.2-fold upregulation of miR-615-3p in hypoxic exosomes (*p <0.01), providing novel mechanistic insights into exosome functional modulation. Functional assays demonstrated superior neuroprotection by hypoxic exosomes compared to Normoxia-Exo, including enhanced

neuronal viability, reduced apoptosis, and ameliorated mitochondrial-ER dysfunction through calcium signaling regulation [34].

In vivo studies confirmed functional recovery in SCI mice receiving Hypo-BMSC-Exo. The observed improvement in BBB locomotor scores—a validated and cornerstone functional outcome measure in rodent SCI models [26]—was not an isolated finding. It was corroborated by increased stride length, reduced lesion volumes, and attenuated inflammatory infiltrates. This convergence of functional improvement (BBB scores) with structural preservation (histopathology) underscores the relevance of our assessment. Moreover, the reduction in tissue edema observed in H&E-stained sections (Fig. 7A-B) suggests that hypoxic exosomes also ameliorate vasogenic edema, a key pathological feature of secondary injury. This in vivo finding indicates that the therapeutic benefits extend beyond direct neuronal protection to encompass the preservation of vascular integrity.Mechanistic investigations revealed that hypoxic exosomes exert neuroprotection through miR-615-3p-mediated PDE4C suppression, activating cAMP/PKA signaling to mitigate mitochondrial calcium overload and ER stress (GRP78 downregulation, $*p < 0.01$). While our findings are consistent with the established roles of microRNAs in intercellular communication [35-38], they uniquely identify the miR-615-3p/PDE4C axis as a critical therapeutic target in SCI.In contrast to broad-spectrum anti-inflammatory strategies, our approach leverages a neuron-specific miRNA-mRNA axis (miR-615-3p/PDE4C) to achieve targeted neuroprotection, offering a distinct and potentially more precise therapeutic mechanism for SCI.

Furthermore, our findings suggest synergistic therapeutic effects from hypoxia-induced exosomal cargo modulation rather than isolated miR-615-3p overexpression. This implies that hypoxia may activate multifactorial protective mechanisms in BMSCs, including growth factor upregulation and anti-apoptotic signaling, which collectively enhance exosome therapeutic potency [39,40].We acknowledge that our reductionist in vitro model, while invaluable for delineating the direct neuron-intrinsic protective role of the miR-615-3p/PDE4C axis, does not fully capture the complex neuron-glia crosstalk and pathologic features like vasogenic edema present in vivo [41]. To bridge this gap and directly investigate the interaction between our neuron-targeted therapy and other key cellular players, future work will employ more complex model systems. Specifically, we plan to utilize neuron-astrocyte microglial co-culture systems, building upon our established primary cell isolation and culture protocols (as detailed in our Methods). Furthermore, spinal cord organotypic slice cultures, which better preserve the native tissue cytoarchitecture and allow for the study of myelin debris effects, will be adopted to validate and extend our findings within an integrated tissue context.Looking further towards clinical translation, the development of robust Chemistry, Manufacturing, and Controls (CMC) strategies will be paramount. Our identification of the miR-615-3p/PDE4C axis provides a mechanistic foundation for developing a potency assay—a critical CMC guardrail. A future assay quantifying miR-615-3p enrichment in hypoxic exosomes and/or functional downregulation of PDE4C in recipient cells could serve as a key quality attribute for standardizing batches and ensuring consistent therapeutic efficacy in preclinical and clinical manufacturing.Nevertheless, the significant functional recovery and attenuated tissue edema

observed in our murine SCI model (Fig. 7A-B) confirm that the therapeutic benefits of hypoxic exosomes effectively translate to the intact spinal cord milieu, extending beyond direct neuronal protection to encompass the preservation of vascular integrity.

It is also noteworthy that hypoxia preconditioning is known to alter the expression of multiple miRNAs and proteins in exosomes, as demonstrated in studies where hypoxic-preconditioned MSC-derived vesicles modulate astrocyte phenotype and promote spinal cord repair [42]. While we focused on miR-615-3p, other hypoxia-induced cargo (e.g., miR-21, miR-210, or heat shock proteins) may synergistically contribute to the observed neuroprotection. Future multi-omics studies are warranted to comprehensively characterize the hypoxic exosomal cargo and elucidate the potential contributions of these molecules.

Despite these advances, several limitations warrant consideration. First, our reductionist in vitro models, while invaluable for delineating the direct neuron-intrinsic protective role of the miR-615-3p/PDE4C axis, do not fully capture the complex neuron-glia crosstalk and pathologic features like vasogenic edema present in vivo. Nevertheless, the significant functional recovery and attenuated tissue edema observed in our murine SCI model (Fig. 7A-B) confirm that the therapeutic benefits effectively translate to the intact spinal cord milieu. Second, while our in vitro and murine models provide compelling mechanistic insights, translational validation in large animal models and clinical trials remains essential to confirm safety and efficacy. Furthermore, our therapeutic approach employed a single, immediate dose of exosomes. Although this regimen was rationalized by established protocols and supported by our IVIS tracking data (Fig. 6A-B),

which confirmed robust exosome accumulation at the lesion site within 24 hours, we recognize that defining the optimal therapeutic window is critical for translation. While preliminary observations from our pilot studies indicated that the immediate (0-hour) administration was effective, systematic investigations into delayed dosing (e.g., 6–24 hours post-injury) and dose-escalation are necessary future steps to fully delineate the treatment window and maximize clinical relevance.Third, although we identify the miR-615-3p/PDE4C axis as a key mechanism, potential contributions from other hypoxia-regulated microRNAs or signaling pathways require investigation. Finally, the present study primarily focused on short-term outcomes (up to 14 days post-injury). This long-term assessment will utilize the same murine SCI model and exosome administration protocols established herein. We will evaluate the durability of motor function recovery using the BBB scale and footprint analysis, monitor animal welfare and body weight for signs of systemic adverse effects, and perform detailed histopathological and molecular analyses on harvested spinal cord tissues to assess lesion maturation, glial scar formation, and the persistence of key molecular markers (e.g., PDE4C, inflammatory cytokines).

Furthermore, while behavioral and histological assessments were conducted with a sample size of 5-8 animals per group, the sample size for molecular analyses (Western blot, qPCR) was n=3 per group due to tissue availability. Although consistent directional trends were observed across these molecular endpoints, future studies with larger sample sizes are warranted to confirm these findings.

Moreover, while we focused on the miR-615-3p/PDE4C axis, it is possible that other miRNAs or signaling pathways modulated by hypoxia may also contribute to the observed effects. Future studies employing multi-omics approaches are needed to comprehensively characterize the cargo of hypoxic exosomes and their synergistic mechanisms.

5. Conclusion

This study investigates the neuroprotective mechanisms of hypoxia-conditioned BMSC exosomes in spinal cord injury (SCI). The results demonstrate that hypoxia significantly enhances the functional capacity of these exosomes, at least partially through miR-615-3p upregulation. These exosomes exert neuroprotective effects by targeting the PDE4C/cAMP/PKA signaling axis, thereby alleviating mitochondrial-ER dysfunction and calcium dysregulation. These findings demonstrate the short-term therapeutic potential of hypoxia-engineered exosomes for SCI within the 14-day post-injury period. However, confirmation of their long-term efficacy and safety in studies extending to 28 days and beyond, alongside validation in larger animal models, is necessary before clinical translation.Additionally, it is important to acknowledge the limitations of this study, including the use of animal models and the lack of long-term efficacy and safety data, which necessitates further investigation to validate the translational relevance to humans. The complex pathophysiology of SCI also suggests that other mechanisms beyond the PDE4C/cAMP/PKA pathway may contribute to the observed neuroprotective effects. Further research is necessary to fully elucidate these mechanisms and evaluate the clinical applicability of hypoxia-engineered exosomes.

Declarations

Funding

This work was supported by the National Natural Science Foundation of China (Grant/Award Number: 81971828). The funder had no role in study design, data collection, analysis, or manuscript preparation.

Conflict of interest

The authors declare no competing interests.

AI Statement

The authors declare that they have not used AI-generated work in this manuscript.

Supplementary Information

The online version contains supplementary material available at Supplementary File 1 (Supplementary Table S1): Detailed list of key reagents and instruments, including suppliers, catalog numbers, RRIDs, and working concentrations/details.

Data Availability

The raw data supporting the findings of this study—including individual BBB scores, raw NTA videos, and uncropped Western blot images—ihave been compiled into a Supplementary Data File submitted for peer review. During the review process, these data are not publicly available due to institutional policy but can be provided by the corresponding author upon reasonable request. If accepted, the authors intend to deposit the data in a public repository such as the Open Science Framework (OSF) or Zenodo,

subject to final institutional approval, and will provide the accession details upon publication.

Ethics approval and consent to participate

All animal experiments were conducted under strict adherence to the Chinese Regulations for the Administration of Laboratory Animals (2017 Revision) and the Harbin Medical University Animal Welfare Guidelines. The study protocol titled "Mechanism of BMSC-Derived Exosomes in Spinal Cord Injury Repair" (Approval Number: SYDW2024-111) was reviewed and approved by the Institutional Animal Care and Use Committee (IACUC) of the Second Affiliated Hospital of Harbin Medical University on 2024-03-15.

Human subjects and samples

This study did not involve human participants, human tissue, or clinical data. All experiments utilized animal models and immortalized human spinal neuronal cell lines (Sciencell #1521). No informed consent or ethical approval for human research was required.

Animal study

Animal welfare and experimental procedures complied with the ARRIVE 2.0 guidelines. For animals designated for histological analysis, euthanasia was performed under deep anesthesia followed by transcardial perfusion with 4% paraformaldehyde to ensure optimal tissue preservation. All procedures were in accordance with the AVMA Guidelines for the Euthanasia of Animals (2020) and approved by the institutional animal care and use committee.

Cell line authentication

The human spinal neuronal cell line (Sciencell #1521) used in this study was commercially sourced and authenticated by short tandem repeat (STR) profiling. No additional ethical approval was required for cell line utilization.

Clinical trial registration

Not applicable. This study did not involve human subjects or clinical interventions.

References

[1]Safdarian M, Trinka E, Rahimi-Movaghar V, et al. Global, regional, and national burden of spinal cord injury, 1990–2019: a systematic analysis for the Global Burden of Disease Study 2019[J]. The Lancet Neurology, 2023, 22(11): 1026-1047.

[2]Baev A Y, Vinokurov A Y, Novikova I N, et al. Interaction of mitochondrial calcium and ROS in neurodegeneration[J]. Cells, 2022, 11(4): 706.

[3]Zhai Q Y, Ye Y H, Ren Y Q, et al. Neuroprotective effects of neural stem cells pretreated with neuregulin1β on PC12 cells exposed to oxygen-glucose deprivation/reoxygenation[J]. Neural Regeneration Research, 2023, 18(3): 618-625.

[4]Rao J, Xie H, Liang Z, et al. Hypoxic-preconditioned mesenchymal stem cell-derived small extracellular vesicles inhibit neuronal death after spinal cord injury by regulating the SIRT1/Nrf2/HO-1 pathway[J]. Frontiers in Pharmacology, 2024, 15: 1419390.

[5]Zhou Q, Meng X, Huang G, et al. MEK1/2 inhibition synergistically enhances the preventive effects of normobaric oxygen on spinal cord injury in decompression sickness rats[J]. Frontiers in Physiology, 2021, 12: 674430.

[6]ANJUM A, YAZID M D I, FAUZI DAUD M, et al. Spinal Cord Injury: Pathophysiology, Multimolecular Interactions, and Underlying Recovery Mechanisms [J]. International Journal of Molecular Sciences, 2020, 21(20).

[7]HACHEM L D, FEHLINGS M G. Pathophysiology of Spinal Cord Injury [J]. Neurosurgery Clinics of North America, 2021, 32(3): 305-13.

[8]Area-Gomez E, Schon E A. Mitochondria-associated ER membranes and Alzheimer disease[J]. Current opinion in genetics & development, 2016, 38: 90-96.

[9]RATURI A, SIMMEN T. Where the endoplasmic reticulum and the mitochondrion tie the knot: the mitochondria-associated membrane (MAM) [J]. Biochim Biophys Acta, 2013, 1833(1): 213-24.

[10]Bhatt M, Sharma M, Das B. The role of inflammatory cascade and reactive astrogliosis in glial scar formation post-spinal cord injury[J]. Cellular and Molecular Neurobiology, 2024, 44(1): 78.

[11]Hu X, Zhang Y, Wang L, et al. Microglial activation in the motor cortex mediated NLRP3-related neuroinflammation and neuronal damage following spinal cord injury[J]. Frontiers in Cellular Neuroscience, 2022, 16: 956079.

[12]Yang R, Yang B, Liu W, et al. Emerging role of non-coding RNAs in neuroinflammation mediated by microglia and astrocytes[J]. Journal of neuroinflammation, 2023, 20(1): 173.

[13]Peng W, Wan L, Luo Z, et al. Microglia-derived exosomes improve spinal cord functional recovery after injury via inhibiting oxidative stress and promoting the survival and function of endothelia cells[J]. Oxidative medicine and cellular longevity, 2021, 2021(1): 1695087.

[14]Venkatesh K, Ghosh S K, Mullick M, et al. Spinal cord injury: pathophysiology, treatment strategies, associated challenges, and future implications[J]. Cell and tissue research, 2019, 377(2): 125-151.

[15]Aldali F, Deng C, Nie M, et al. Advances in therapies using mesenchymal stem cells and their exosomes for treatment of peripheral nerve injury: state of the art and future perspectives[J]. Neural Regeneration Research, 2025, 20(11): 3151-3171.

[16]Han Y, Seyfried D, Meng Y, et al. Multipotent mesenchymal stromal cell–derived exosomes improve functional recovery after experimental intracerebral hemorrhage in the rat[J]. Journal of neurosurgery, 2018, 131(1): 290-300.

[17]Lin M, Alimerzaloo F, Wang X, et al. Harnessing stem cell-derived exosomes: a promising cell-free approach for spinal cord injury[J]. Stem Cell Research & Therapy, 2025, 16(1): 182.

[18]You Y, Tian Y, Guo R, et al. Extracellular vesicle-mediated VEGF-A mRNA delivery rescues ischaemic injury with low immunogenicity[J]. European Heart Journal, 2025: ehae883.

[19]Islam F, Bepary S, Nafady M H, et al. Polyphenols targeting oxidative stress in spinal cord injury: current status and future vision[J]. Oxidative Medicine and Cellular Longevity, 2022, 2022(1): 8741787.

[20]Luan Z, Liu J, Li M, et al. Exosomes derived from umbilical cord-mesenchymal stem cells inhibit the NF-κB/MAPK signaling pathway and reduce the inflammatory response to promote recovery from spinal cord injury[J]. Journal of orthopaedic surgery and research, 2024, 19(1): 184.

[21]Pedro K M, Fehlings M G. Progress and future directions in spinal cord injury trials[J]. The Lancet Neurology, 2025, 24(1): 3-5.

[22]Sheng J, Zhang S, Wu L, et al. Inhibition of phosphodiesterase: A novel therapeutic target for the treatment of mild cognitive impairment and Alzheimer's disease[J]. Frontiers in aging neuroscience, 2022, 14: 1019187.

[23]Schepers M, Vanmierlo T. Novel insights in phosphodiesterase 4 subtype inhibition to target neuroinflammation and stimulate remyelination[J]. Neural regeneration research, 2024, 19(3): 493-494.

[24]Xin H, Liu Z, Buller B, et al. MiR-17-92 enriched exosomes derived from multipotent mesenchymal stromal cells enhance axon-myelin remodeling and motor electrophysiological recovery after stroke[J]. Journal of Cerebral Blood Flow & Metabolism, 2021, 41(5): 1131-1144.

[25]Huang J H, Xu Y, Yin X M, et al. Exosomes derived from miR-126-modified MSCs promote angiogenesis and neurogenesis

and attenuate apoptosis after spinal cord injury in rats[J]. Neuroscience, 2020, 424: 133-145.

[26]Sharif-Alhoseini M, Khormali M, Rezaei M, et al. Animal models of spinal cord injury: a systematic review[J]. Spinal cord, 2017, 55(8): 714-721.

[27]Li Y, Wang Q, Zhang Y, et al. The roles of microRNAs in CNS development and regeneration of spinal cord injury[J]. Journal of Cellular Biology, 2021, 12(4): 123-132.

[28]Long R, Wang S. Exosomes from preconditioned mesenchymal stem cells: Tissue repair and regeneration. Regenerative Therapy, 2024, 25: 355-366.

[29]Gorgun C, Ceresa D, Lesage R, et al. Dissecting the effects of preconditioning with inflammatory cytokines and hypoxia on the angiogenic potential of mesenchymal stromal cell (MSC)-derived soluble proteins and extracellular vesicles (EVs). Biomaterials, 2021, 269: 120633.

[30]Wang K, Jiang Z, Webster K A, et al. Enhanced cardioprotection by human endometrium mesenchymal stem cells driven by exosomal microRNA-21[J]. Stem cells translational medicine, 2017, 6(1): 209-222.

[31]WANG L, LIU Y, ZHANG X, et al. Endoplasmic Reticulum Stress and the Unfolded Protein Response in Cerebral Ischemia/Reperfusion Injury [J]. Front Cell Neurosci, 2022, 16: 864426.

[32]ZHANG Z, MESZAROS G, HE W T, et al. Protein kinase D at the Golgi controls NLRP3 inflammasome activation [J]. J Exp Med, 2017, 214(9): 2671-93.

[33]Pulido-Escribano V, Torrecillas-Baena B, Camacho-Cardenosa M, et al. Role of hypoxia preconditioning in therapeutic potential of mesenchymal stem-cell-derived extracellular vesicles. World Journal of Stem Cells, 2022, 14(7): 453.

[34]Mao C Y, Zhang T T, Li D J, et al. Extracellular vesicles from hypoxia-preconditioned mesenchymal stem cells alleviates myocardial injury by targeting thioredoxin-interacting protein-mediated hypoxia-inducible factor-1α pathway. World Journal of Stem Cells, 2022, 14(2): 183.

[35]Park M, Shin H A, Duong V A, et al. The role of extracellular vesicles in optic nerve injury: neuroprotection and mitochondrial homeostasis. Cells, 2022, 11(23): 3720.

[36]Feng J, Zhang Y, Zhu Z, et al. Emerging exosomes and exosomal MiRNAs in spinal cord injury. Frontiers in cell and developmental biology, 2021, 9: 703989.

[37]Sintakova K, Romanyuk N. The role of small extracellular vesicles and microRNA as their cargo in the spinal cord injury pathophysiology and therapy. Frontiers in Neuroscience, 2024, 18: 1400413.

[38]Huang J H, Yin X M, Xu Y, et al. Systemic administration of exosomes released from mesenchymal stromal cells attenuates apoptosis, inflammation, and promotes angiogenesis after spinal cord injury in rats[J]. Journal of neurotrauma, 2017, 34(24): 3388-3396.

[39]Rani S, Ryan A E, Griffin M D, et al. Mesenchymal stem cell-derived extracellular vesicles: toward cell-free therapeutic applications[J]. Molecular therapy, 2015, 23(5): 812-823.

[40]Ge L, Xun C, Li W, et al. Extracellular vesicles derived from hypoxia-preconditioned olfactory mucosa mesenchymal stem cells enhance angiogenesis via miR-612. Journal of Nanobiotechnology, 2021, 19: 1-23.

[41]Liddelow S A, Guttenplan K A, Clarke L E, et al. Neurotoxic reactive astrocytes are induced by activated microglia[J]. Nature, 2017, 541(7638): 481-487.

[42]Yang Z, Liang Z, Rao J, et al. Hypoxic-preconditioned mesenchymal stem cell-derived small extracellular vesicles promote the recovery of spinal cord injury by affecting the phenotype of astrocytes through the miR-21/JAK2/STAT3 pathway. CNS Neuroscience & Therapeutics, 2024, 30(3): e14428.

Figure legends

Figure 1. Effect of Hypoxia Treatment on BMSC Exosome Characteristics and miR-615-3p Expression.

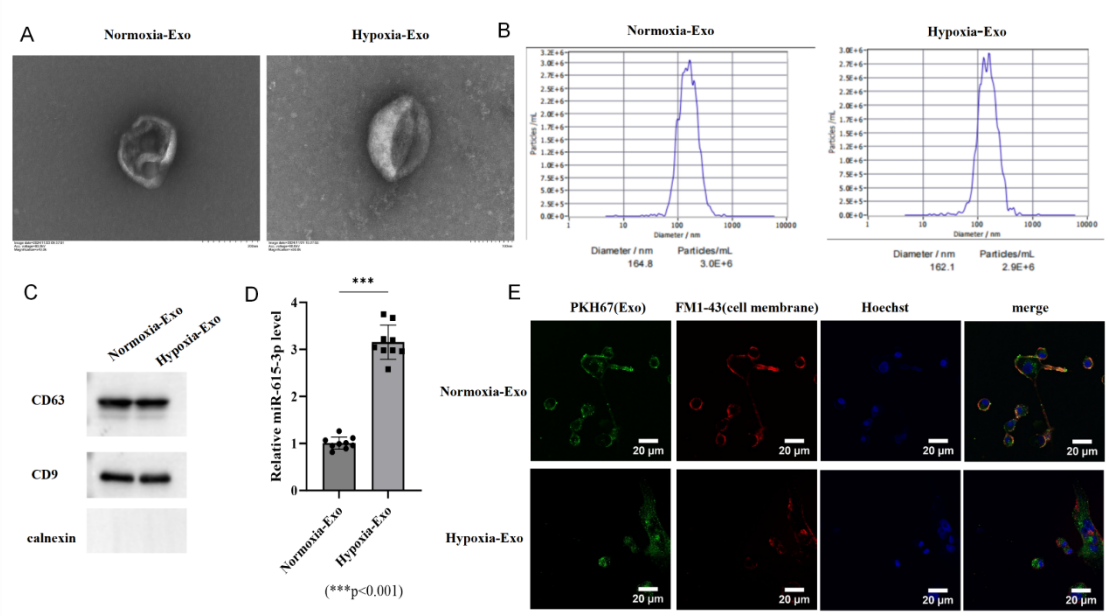

A. Representative transmission electron microscopy (TEM) images of BMSC-derived exosomes from normoxic (left) and hypoxic (right) conditions, showing the characteristic cup-shaped morphology. Scale bar, 100 nm.

B. Nanoparticle tracking analysis (NTA) showing the size distribution profile of exosomes isolated from hypoxic BMSCs. The x-axis represents particle size (nm), and the y-axis represents concentration (particles/mL). The peak particle size is indicated.

C. Western blot analysis of exosomal markers CD63 and CD9, and the negative marker calnexin, in exosomes derived from normoxic (N) and hypoxic (H) BMSCs.

D. Quantitative PCR (qPCR) analysis of miR-615-3p expression in exosomes derived from normoxic (Normoxia-Exo) and hypoxic (Hypoxia-Exo) BMSCs, and in BMSCs cultured under normoxic or hypoxic conditions. Data are presented as mean ± SD with individual data points overlaid (n = 3 independent biological experiments; each point represents one experiment). $^{**}p < 0.01$ vs. Normoxia-Exo group; $^{***}p < 0.001$ vs. Normoxia group (Student's

t-test). The y-axis represents relative expression normalized to U6 snRNA.

E. Confocal microscopy images showing the uptake of PKH67 (green)-labeled hypoxic BMSC-derived exosomes by spinal neurons (nuclei stained with DAPI in blue). Scale bar, 20 μm.

Figure 2. Regulation of miR-615-3p Expression and Exosome Characteristics Verification.

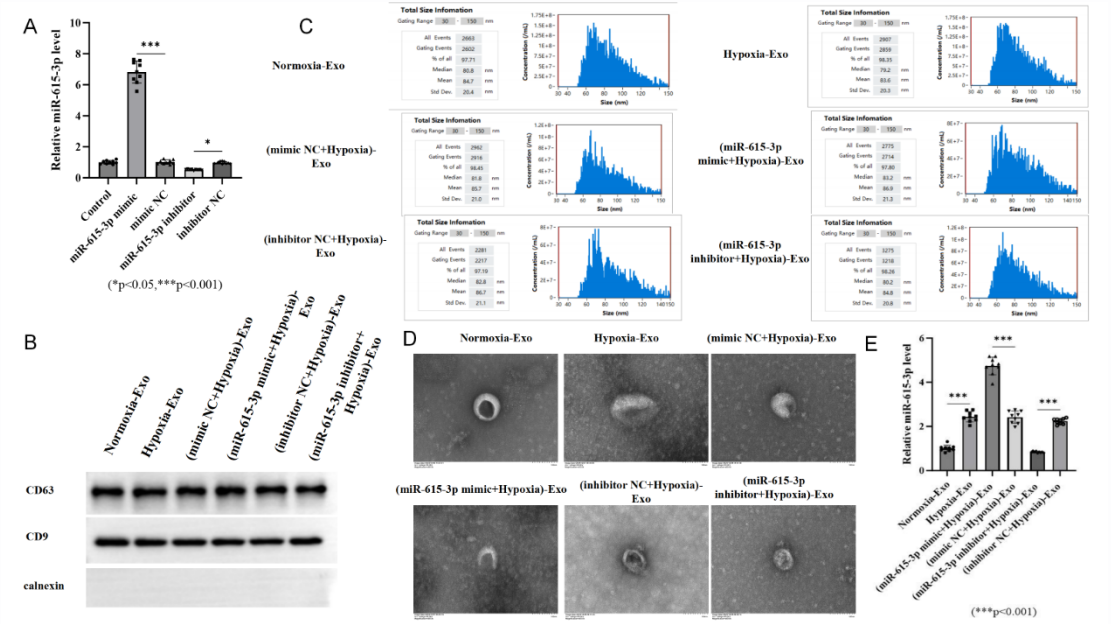

A. qPCR analysis of miR-615-3p expression in BMSCs following transfection with miR-615-3p mimic or inhibitor. Data are presented as mean ± SD with individual data points overlaid (n = 3 independent biological experiments; each point represents one experiment). The y-axis represents relative expression. ***$P <$ 0.001 vs. NC (Negative Control) group (One-way ANOVA).

B. Western blot analysis of exosomal markers (CD63, CD9) and calnexin in exosomes from different treatment groups.

C. Nanoparticle tracking analysis (NTA) showing the size distribution profile of exosomes. The x-axis represents particle size (nm), and the y-axis represents concentration (particles/mL).

D. Representative TEM images of exosomes from each group, verifying the reliability of the exosome extraction method. Scale bar, 100 nm.

E. qPCR detection of miR-615-3p expression in BMSC-derived exosomes after hypoxia induction and miR-615-3p mimic/inhibitor transfection. Data are presented as mean ± SD with individual data points overlaid (n = 3 independent biological experiments; each point represents one experiment). *$p < 0.05$, **$p < 0.01$, ***$p < 0.001$ (One-way ANOVA).

Figure 3. Protective Effect of Hypoxic Exosomes on Spinal Neuronal Cell Viability.

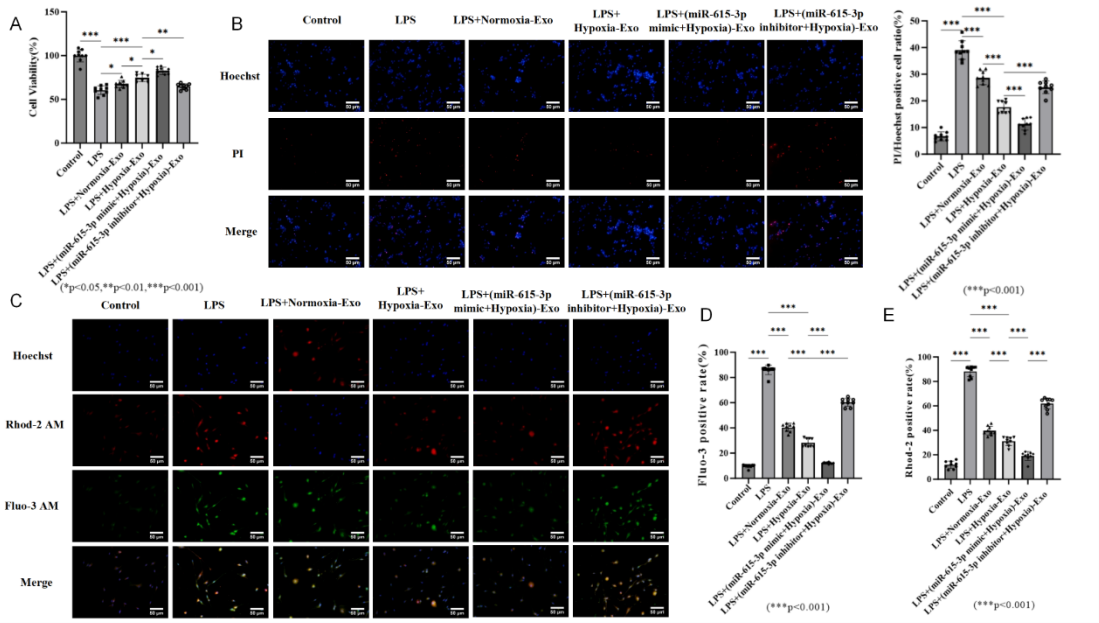

A. Cell viability of spinal neurons assessed by CCK-8 assay after treatment with Normoxia-Exo or Hypoxia-Exo (100 μg/mL) following H_2O_2 injury. Data are presented as mean ± SD with

individual data points overlaid (n = 6 independent culture wells; each point represents one well). The y-axis represents cell viability (% of control). ***$p < 0.001$ vs. H_2O_2 + Normoxia-Exo group (One-way ANOVA with Bonferroni's post hoc test).

B. Representative fluorescence images of spinal neurons stained with Hoechst 33342 (blue, all nuclei) and propidium iodide (PI, red, dead cells) after the indicated treatments. Scale bar, 50 μm.

C. Cytosolic calcium levels in spinal neurons measured by Fluo-3 AM fluorescence intensity (in arbitrary units, A.U.) after the indicated treatments. Data are presented as mean ± SD with individual data points overlaid (n = 3 independent experiments, with at least 30 cells analyzed per experiment). **$p < 0.05$, ***$p < 0.01$ vs. H_2O_2 + Normoxia-Exo group (One-way ANOVA with Bonferroni's post hoc test). Right panel: Representative fluorescence images. Scale bar, 20 μm.

D. Mitochondrial calcium levels in spinal neurons measured by Rhod-2 AM fluorescence intensity after the indicated treatments. Data are presented as mean ± SD with individual data points overlaid (n = 3 independent experiments, with at least 30 cells analyzed per experiment). The y-axis represents fluorescence intensity in arbitrary units (A.U.).**$p < 0.05$, ***$p < 0.01$ vs. H_2O_2 + Normoxia-Exo group (One-way ANOVA with Bonferroni's post hoc test). Right panel: Representative fluorescence images. Scale bar, 20 μm.

Figure 4. Improvement of Mitochondrial-Endoplasmic Reticulum Contact Site Structure Integrity by Hypoxic Exosomes.

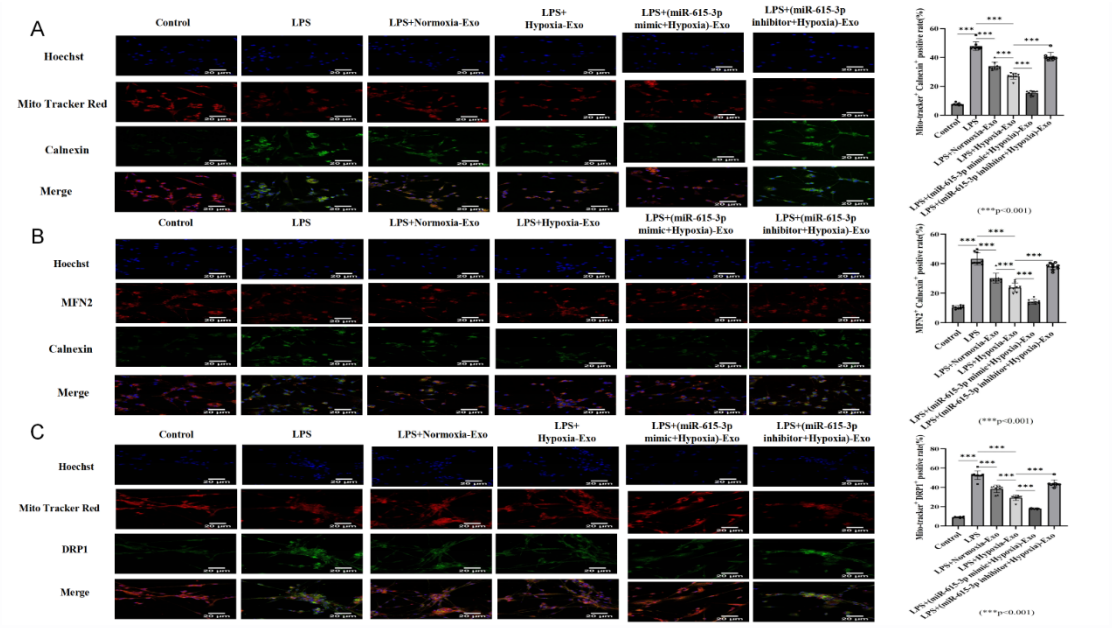

A-C. Representative confocal microscopy images and quantitative analysis of mitochondrial-ER associated membranes (MAMs) in spinal neurons.

A. Immunofluorescence staining for mitochondria (MitoTracker Red, red) and endoplasmic reticulum (Anti-Calnexin antibody, green). Yellow areas in the merged images indicate MAMs. Scale bar, 5 μm. The graph shows the quantification of MAMs integrity (Pearson's correlation coefficient). Data are presented as mean ± SD with individual data points overlaid (n = 3 independent experiments; each point represents the mean value from one experiment, with at least 15 cells analyzed per experiment). $^{**}p < 0.01$ vs. H_2O_2 + Normoxia-Exo group (One-way ANOVA).

B. Colocalization analysis of mitofusin 2 (MFN2, green) with MAMs (labeled by Calnexin, red). The graph shows the Manders' colocalization coefficient for MFN2. Data are presented as mean ± SD with individual data points overlaid. $^{**}p < 0.01$ vs. H_2O_2 + Normoxia-Exo group.

C. Colocalization analysis of dynamin-related protein 1 (DRP1, green) with mitochondria (labeled by MitoTracker Red, red). The graph shows the Manders' colocalization coefficient for DRP1. Data are presented as mean ± SD with individual data points overlaid. *$p < 0.05$ vs. H_2O_2 + Normoxia-Exo group.

Figure 5. Regulation of Oxidative Stress, Inflammatory Factors, and Gene Expression by Hypoxic Exosomes.

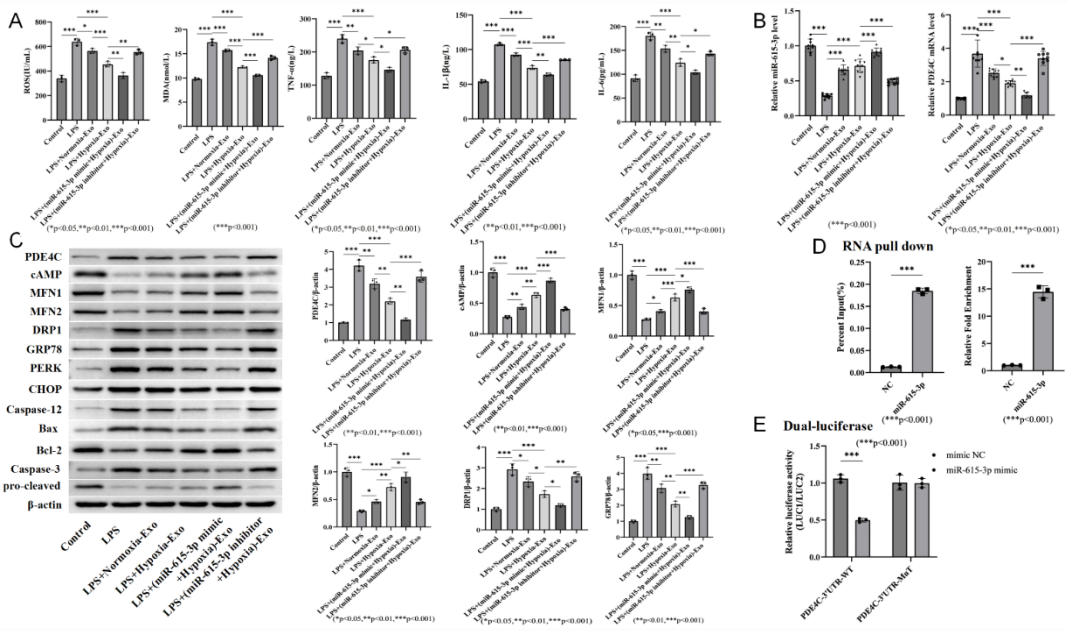

A. ELISA quantification of reactive oxygen species (ROS) and the pro-inflammatory cytokine TNF-α in the culture supernatant of spinal neurons after the indicated treatments. Data are presented as mean ± SD with individual data points overlaid (n = 3 independent biological experiments; each point represents one experiment). The y-axis for ROS represents fluorescence intensity (A.U.); for TNF-α, it represents concentration (pg/mL). *$p < 0.05$, **$p < 0.01$ vs. H_2O_2 + Normoxia-Exo group (One-way ANOVA).

B. qPCR analysis of miR-615-3p and PDE4C mRNA expression in spinal neurons after the indicated treatments. Data are presented as mean ± SD with individual data points overlaid (n = 3

independent biological experiments; each point represents one experiment). The y-axis represents relative expression. *$p < 0.05$, **$p < 0.01$ vs. H_2O_2 + Normoxia-Exo group (One-way ANOVA).

C. Western blot analysis of PDE4C protein expression in spinal neurons after the indicated treatments. GAPDH served as a loading control.

D. RNA pull-down assay using a biotinylated miR-615-3p mimic and its corresponding mutant (Mut). The pulled-down RNA was subjected to qPCR for PDE4C. Data are presented as mean ± SD with individual data points overlaid (n = 3 independent biological experiments; each point represents one experiment). *$p < 0.05$ vs. Mut group (Student's t-test).

E. Dual-luciferase reporter assay in HEK293T cells co-transfected with a wild-type (WT) or mutant (Mut) PDE4C 3'UTR reporter plasmid and miR-615-3p mimic or negative control (NC). Firefly luciferase activity was normalized to Renilla luciferase. Data are presented as mean ± SD with individual data points overlaid (n = 3 independent biological experiments; each point represents one experiment). The y-axis represents relative luciferase activity. *$p <$ 0.05 vs. NC mimic group (Student's t-test).

Figure 6. Promotion of Motor Function Recovery in Spinal Cord Injury Mice by Hypoxic Exosomes.

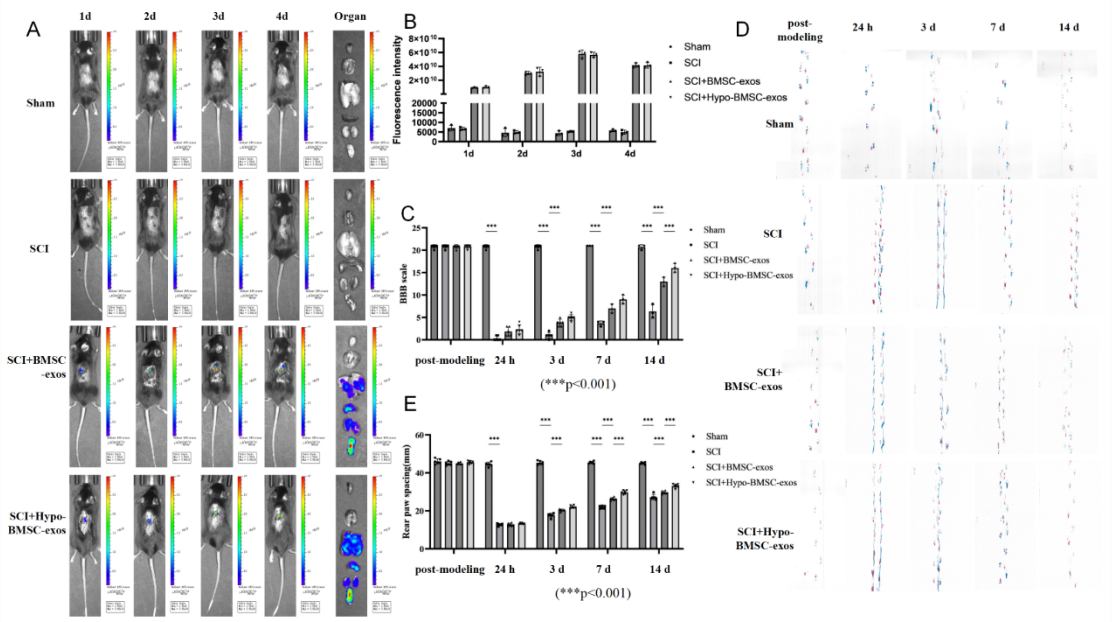

A-B. In vivo imaging system (IVIS) tracking of DiR-labeled exosomes at 24 hours post-injection via tail vein. (A) Representative images showing exosome biodistribution. (B) Quantitative fluorescence intensity at the spinal cord injury site. Data are presented as mean ± SD with individual data points overlaid (n = 5 mice per group). The y-axis represents radiant efficiency ([p/s/cm²/sr]/[μW/cm²]). *$p < 0.05$ vs. Normoxia-Exo group (Student's t-test).

C. Time course of hindlimb locomotor recovery assessed by the Basso, Beattie, Bresnahan (BBB) scale following SCI and exosome treatment. Data are presented as mean ± SD with individual data points overlaid (n = 8 mice per group). The y-axis represents BBB score. *p < 0.05, **p < 0.01 vs. SCI + PBS group at the corresponding time point (Two-way repeated measures ANOVA with Bonferroni's post hoc test).

D-E. Footprint analysis of gait function on post-injury day 14.

D. Quantitative analysis of hindpaw stride length. Data are presented as mean ± SD with individual data points overlaid (n = 8

mice per group; each point represents one animal). The y-axis represents stride length (mm). **$p < 0.01$ vs. SCI + PBS group (One-way ANOVA).

E. Representative footprint patterns from each treatment group. Forepaws (red) and hindpaws (blue).

Figure 7. Hypoxic Exosomes Ameliorate Histopathological Damage after Spinal Cord Injury.

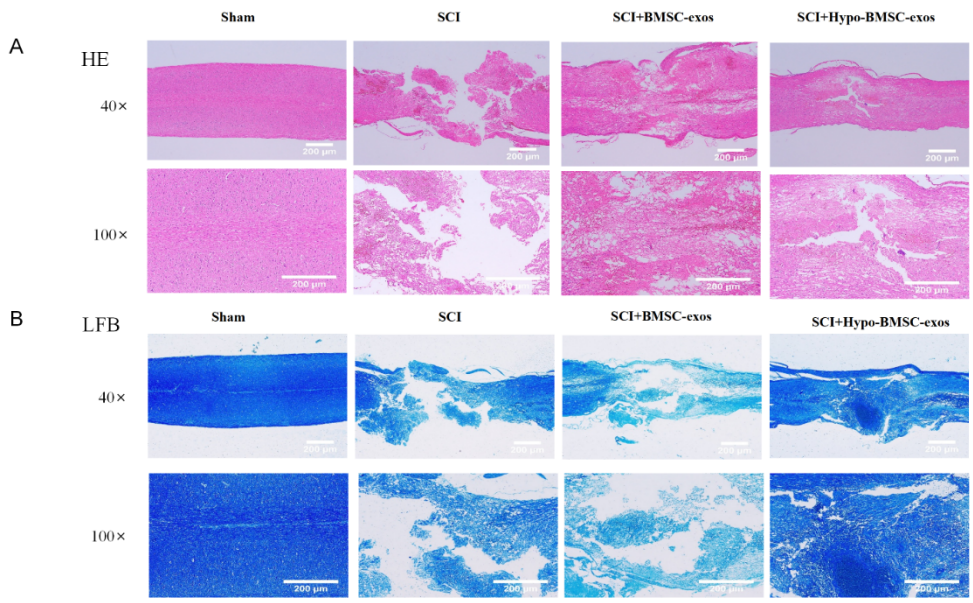

A. Representative hematoxylin and eosin (H&E)-stained longitudinal sections of the spinal cord (paraffin-embedded, 4 µm) at the lesion epicenter on post-injury day (PID) 14. The graph shows the quantitative analysis of the lesion area. Data are presented as mean ± SD with individual data points overlaid (n = 5 mice per group). The y-axis represents lesion area (mm^2). **$p <$ 0.01 vs. SCI + PBS group (One-way ANOVA with Bonferroni's post hoc test).

B. High-magnification views of the boxed regions in (A) and quantitative analysis of infiltrating inflammatory cells per high-power field (HPF, 400x magnification). Hypoxic exosome

treatment reduced inflammatory cell infiltration (indicated by arrows). Data are presented as mean ± SD with individual data points overlaid (n = 5 mice per group, 3 HPFs per mouse). The y-axis represents number of inflammatory cells per HPF. *$p < 0.05$ vs. SCI + PBS group (One-way ANOVA with Bonferroni's post hoc test).

Figure 8. Hypoxic Exosomes Regulate SCI-Related Molecular Expression and Oxidative Stress in Vivo.

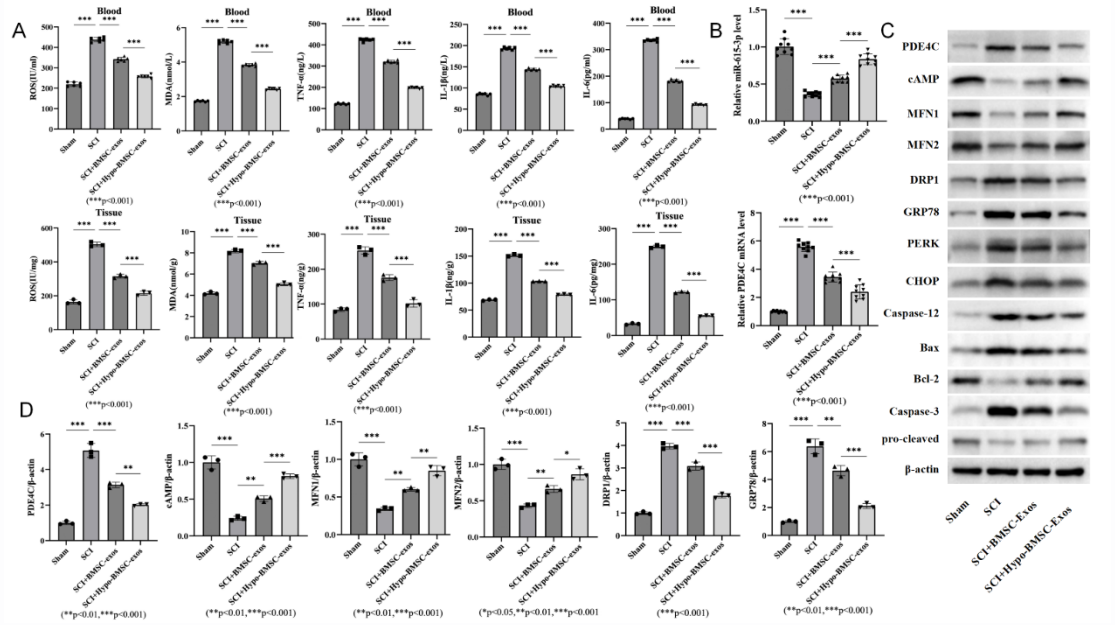

A. ELISA quantification of oxidative stress marker Malondialdehyde (MDA) and pro-inflammatory cytokines (TNF-α, IL-6) in spinal cord homogenates or serum on PID 3. Data are presented as mean ± SD with individual data points overlaid (n = 5 mice per group). The y-axis for MDA represents concentration (nmol/mg prot); for cytokines, it represents concentration (pg/mL). *$p < 0.05$, **$p < 0.01$ vs. SCI + PBS group (One-way ANOVA with Bonferroni's post hoc test).

B. Quantitative PCR (qPCR) analysis of miR-615-3p and PDE4C mRNA expression in spinal cord tissues surrounding the lesion site

on PID 3. Data are presented as mean ± SD with individual data points overlaid (n = 5 mice per group). The y-axis represents relative expression. *$p < 0.05$, **$p < 0.01$ vs. SCI + PBS group (One-way ANOVA with Bonferroni's post hoc test).

C. Representative Western blot images and densitometric quantification of PDE4C protein expression in spinal cord tissues on PID 3, normalized to GAPDH. Each data point represents an individual animal. Data are presented as mean ± SD with individual data points overlaid (n = 3 biologically independent animals per group). The y-axis represents relative protein expression. The y-axis represents relative protein expression. *$p < 0.05$ vs. SCI + PBS group (One-way ANOVA with Bonferroni's post hoc test).

D. Representative Western blot images and quantification of the phosphorylated PKA to total PKA (p-PKA / t-PKA) ratio and GRP78 protein expression in spinal cord tissues on PID 3. Each data point represents an individual animal. Data are presented as mean ± SD with individual data points overlaid (n = 3 biologically independent animals per group). The y-axis represents relative ratio or expression. *$p < 0.05$, **$p < 0.01$ vs. SCI + PBS group (One-way ANOVA with Bonferroni's post hoc test).